

Problems with twilight/supersky flat-field for wide-field robotic telescopes and the solution

Peng Wei¹, Zhaohui Shang^{2,1}, Bin Ma¹, Cheng Zhao³,
Yi Hu¹, Qiang Liu¹

¹National Astronomical Observatories, Chinese Academy of Sciences, Beijing, China;

²Tianjin Normal University, Tianjin, China;

³Tsinghua University, Beijing, China;;

ABSTRACT

Twilight/night sky images are often used for flat-fielding CCD images, but the brightness gradient in twilight/night sky causes problems of accurate flat-field correction in astronomical images for wide-field telescopes. Using data from the Antarctic Survey Telescope (AST3), we found that when the sky brightness gradient is minimum and stable, there is still a gradient of 1% across AST3's field-of-view of 4.3 square degrees. We tested various approaches to remove the varying gradients in individual flat-field images. Our final optimal method can reduce the spatially dependent errors caused by the gradient to the negligible level. We also suggest a guideline of flat-fielding using twilight/night sky images for wide-field robotic autonomous telescopes.

Keywords: Wide-field Robotic Telescopes, Flat-field, Antarctica Astronomy, AST3

1. INTRODUCTION

For modern observational astronomy, flat-field correction is a necessary and critical step in data processing, which directly affects the accuracy of photometry. A flat-field correction aims to correct the non-uniform response of the optical system and the detector, so the uniformity of the light source (a screen illuminated by a lamp, or twilight/dark night sky) is crucial for the effectiveness of the flat-field correction.

On the one hand, for wide-field robotic autonomous telescopes, due to the wide field-of-view, the gradient in the surface brightness of the twilight/dark night sky becomes a problem. In addition, the difference of the gradient between different flat-field images affects the combined master image precision and leaves some large-scale structures in the master flat-field. These large-scale structures introduce systematic errors into the photometry.

On the other hand, obtaining a dome flat-field for robotic telescopes automatically has a higher level of technology costs, due to its special design (usually compact dome or no dome) and its highly automated operation without human intervention.

A typical field-of-view of photometric telescopes mostly cover 5–10 arcminutes on the sky. The surface brightness distribution of the twilight/night sky in such a small size is sufficient to provide uniform illumination for flat-field correction. However, large sky surveys require large field-of-view for survey efficiency and there have been many telescopes with a field-of-view much larger than 1 square degree. Therefore the flat-field correction for wide-field telescopes must take into account the non-uniform surface brightness of the twilight/night sky light seriously. For the twilight sky, previous studies have found that there is a brightness gradient of 2%–5% per degree under a typical twilight sky observing condition.^{1,2} And several correlations have been found between this gradient and observing time (i.e., solar altitude) as well as the relative position between the sun and the field-of-view where telescope points.^{1,3} Even the dark night sky which is conventionally used to test the flat-field flatness also becomes non-uniform on a large scale (e.g., 1 sq. degrees).⁴ If the sky flat-field images with stochastic gradients are combined to create a master flat-field or supersky flat, its accuracy and flatness will decline, but there has been little study on this issue for large field-of-view telescopes.

Send correspondence to Zhaohui Shang: zshang@gmail.com

This work is based on large amounts of sky flat-field data taken by the Antarctic Survey Telescope (AST3). AST3 consists of three wide-field 0.5/0.68m modified Schmidt telescopes with f-ratio $f/3.73$.^{5,6} These catadioptric telescopes were designed for wide field-of-view (4.3 sq. degrees) survey with a shorter tube than traditional Schmitt telescope. They are equipped with a large single-chip 10Kx10K CCD operated in frame transfer mode with an effective exposure area of 10Kx5K and 16 readout channels. On the focal plane with the plane scale of 1 arcsecond per pixel, this corresponds to 4.3 sq. degrees (1.47 deg x 2.93 deg). The thermoelectric cooling (TEC) module is used to cool the CCD chip to below the environmental temperature at Dome A in the winter, which is about $-60^{\circ}C$ on average.

By analyzing the flat-field data from the AST3, we aim at 1) investigating the uniformity of the sky brightness, the spatial distribution of the sky brightness and its variation with time, 2) analyzing and comparing various components in flat-field and 3) studying and optimizing the flat-field acquisition strategies and the automatic observation procedures.

2. OBSERVATION AND DATA

In January 2012, the first AST3 (AST3-1) equipped with the SDSS i' -band filter was installed at Dome A, the highest place of the Antarctic Plateau.⁷ When the polar day ended on 15 March, AST3-1 began to acquire images. Unfortunately, it stopped working on May 8th because of a problem in the power supply system. During the 56 day observing period, we obtained more than 22,000 images, including 2,451 sky flat-field images.

We select the images with sky brightness in the middle of the dynamic range of the CCD, between 15,000 and 30,000 ADU. The lower limit is to ensure high S/N and the upper limit is to avoid non-linear response of the CCD near saturation. We also discard the flat-field images taken with high CCD temperatures above $-40^{\circ}C$, because the high-level dark current at these temperatures is hard to correct perfectly. The average CCD temperature at which the rest of the images were taken is $-60^{\circ}C$, which corresponds to a dark current of only 1 ADU/s. Then we also require all images to have a sky flux larger than 100 ADU/s so that the dark current correction is small and does not introduce much noise.

Finally, there are 906 flat-field images left for analysis and their average sky brightness is 22,500 ADU.

3. GRADIENTS IN THE SKY BRIGHTNESS

The original images of our sample have been pre-processed with a series of steps, such as crosstalk correction (crosstalk phenomenon: the multi-channel CCD readout inter-channel interference), overscan correction, and dark current correction. Finally, they are normalized and we have many individual-exposure pre-processed flat-field image F_i .

We take image a0425.810.fit as an example (Fig. 1). As we can see, except for pixel-to-pixel nonuniform structure, there are multiple large-scale structures in the individual flat-field image, such as the vignetting and the obvious different mean values of each readout channel due to different amplifier gains. These all need to be corrected by the final flat field correction. However, in order to derive the brightness gradient, we need to remove these large-scale effects first, otherwise they can hide the brightness gradients and make them hard to correct. To do this, we apply an initial master flat-field correction to individual images.

We combined those pre-processed images to obtain the initial master flat-field by median stacking. Then each individual flat-field image is divided by this master flat-field. The resulted images consist chiefly of the gradient component relative to the gradient of the initial master flat-field. Because of the median stacking combination, the gradient in the initial master flat-field is small. Also since we focus on correcting the pixel-to-pixel variation in the flat field, the large-scale gradient in the initial master flat-field does not affect our final results. Then we fitted the individual resulted image with a two-dimensional inclined plane $Z = a + bX + cY$ and derived the relative gradient $G_i = \sqrt{b^2 + c^2}$.

We check how the position of the Sun affects the twilight flat-field images. As expected, we found a close relationship between the sky brightness $Flux_{sky}$ and solar altitude (see Fig. 2). We fit this relationship and obtain an empirical function:

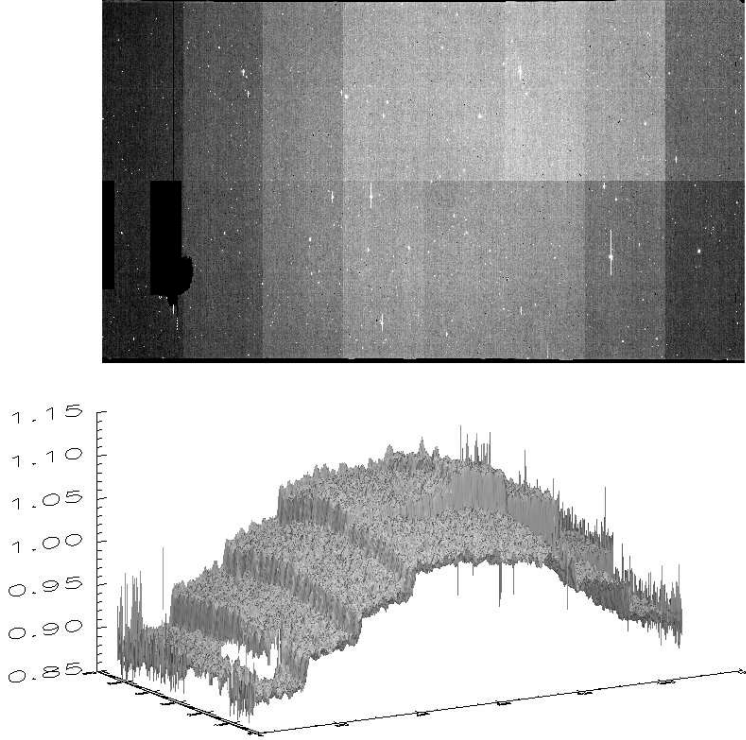


Figure 1. The 2d and 3D plots of raw image a0425.810.fit, a flat-field frame taken by AST3-1. The black regions in lower-left part of the image are the bad pixels which were masked.

$$Flux_{sky} = 10^{0.415alt_{sun}+5.926} \tag{1}$$

We also found that the sky brightness gradients of each frame G_i is related to the azimuth angle θ_i between the telescope pointing and the Sun (Fig. 3). The empirical function from the fitting can be written as:

$$G_i = 10^{-0.00486\theta_i+1.939} \tag{2}$$

These relationships confirm those in the previous studies about twilight sky and the steady state “standard model” of Earth’s atmosphere^{1,3,8}.

4. REMOVE GRADIENTS AND CONSTRUCT A MASTER FLAT-FIELD

To build the final master flat-field, we have further rejected images which have large gradient or large fitting residuals, because the vast majority of them have interference structure due to the presence of cirrus or scatter light. We have also discarded the images containing significant star-trailing due to telescope tracking problem during the exposure. The final sample has 200 images.

In order to minimize the spatially dependent photometric errors, we need to fit and remove the gradients in these 200 individual flat-field frames before combining them. Previous research¹ have found that the wide-field frames should display a linear gradient in the sky background. But by checking our images, we found that the non-uniform structure is more complex than a simple linear inclined plane. In addition, there are some instant Gain changes between channels due to the instability of the amplifiers. So instead of fitting the full frame, we choose to fit each channel. This method will introduce more degree of freedom for fitting. Eventually, to remove the gradient, we simply divide each image by its fit.

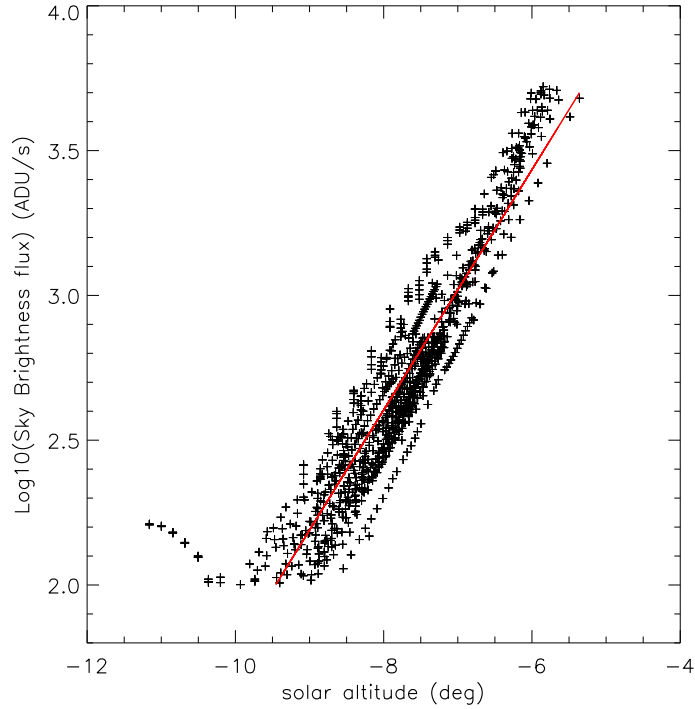


Figure 2. The correlation between the sky brightness and solar altitude for each individual flat-field frame in our sample. The solid line indicates the best fit. By checking the images, we found that the weird tail with the solar altitude below -10° are caused by the moonlight when the scattering sunlight did not dominate the sky brightness during full moon.

In general, our method to remove the gradient in the flat-field images and obtain the final master flat-field can be expressed as:

$$MasterFlat = median_comb \left(\frac{F_i}{fitting(\frac{F_i}{median_comb(F_i)})} \right). \quad (3)$$

where i denotes the i th image. The *mediani_comb()* function means the result from combining all images and the *fitting()* function means the fitting result and operates on each individual image. The fitting is actually applied to each channel of an image with a 2D plane defined as $Z = a + bX + cZ$. The parameter a can reflect the channel Gain variation relative to the initial master flat-field. Our fitting method can correct this variation that otherwise introduces errors in combination of images.

We show an example of image a0425.810.fit in Fig. 4, including the image after divided by the initial master flat-field, fitting result with the full-frame fitting, and fitting result with the channel fitting. We note that the full-frame fitting does not account for the extra change in the Gain of each channel.

To estimate the errors from this method, we also construct the RMS image when combining the 200 individual flat-field images to the master flat-field. Fig 5 shows the RMS images with and without the gradient correction. It is clear that obtaining the master flat-field after the gradient correction results in a much smaller RMS. We also note that the difference between full-frame fitting and channel fitting is not big, the master flat-fields of both have a final mean RMS of 0.1-0.2%, but the channel fitting method can reduce the spatial error in the combined master flat-field to the negligible level compared to the photon noise.

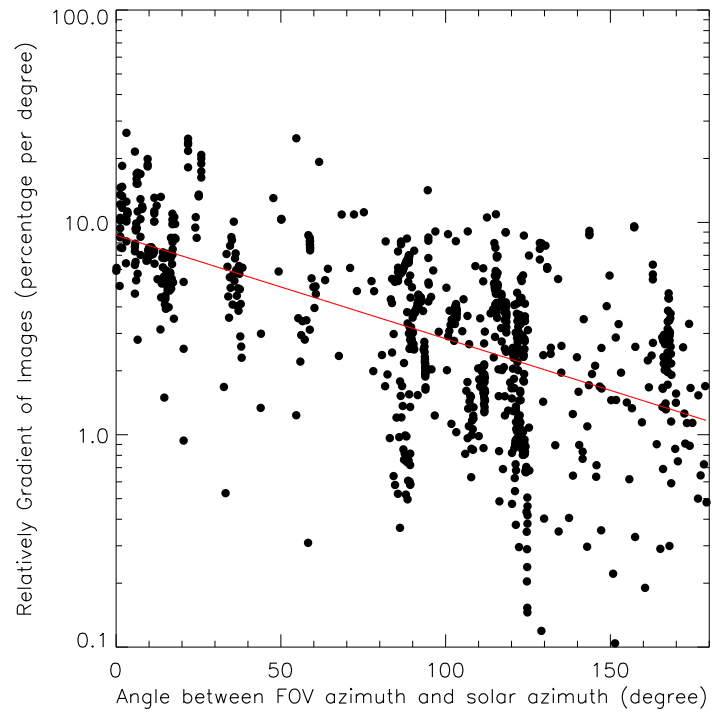


Figure 3. The gradient of sky brightness as a function of the angle between telescope pointing azimuth and solar azimuth. Every data point represents one individual flat-field frame in our sample. The solid line indicates the best fit.

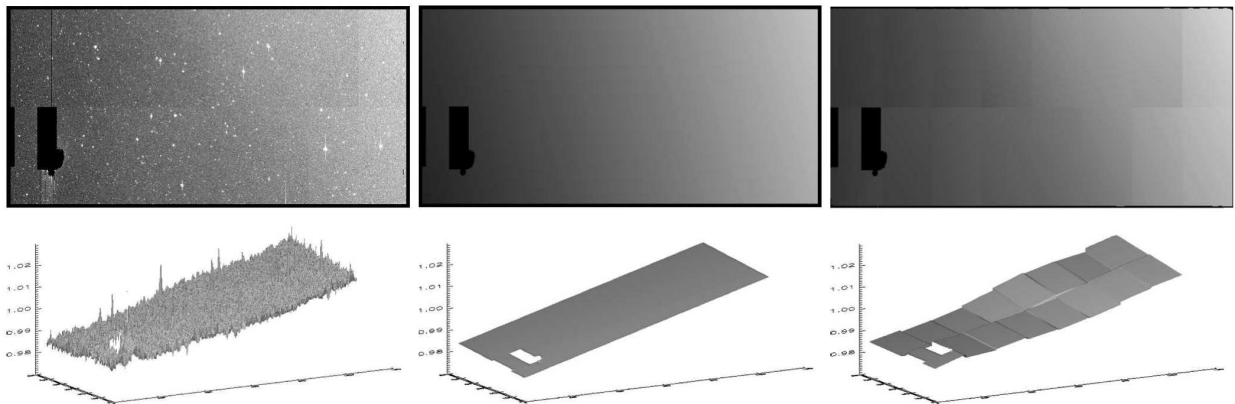


Figure 4. Left: 2D and 3D plots of the flat-field corrected image of a0425.810.fit using the initial master flat; Middle: the full-frame fitting result of the left image; Right: the channel fitting result of the left image. The black regions in the lower-left part of each image are the bad pixels which were masked.

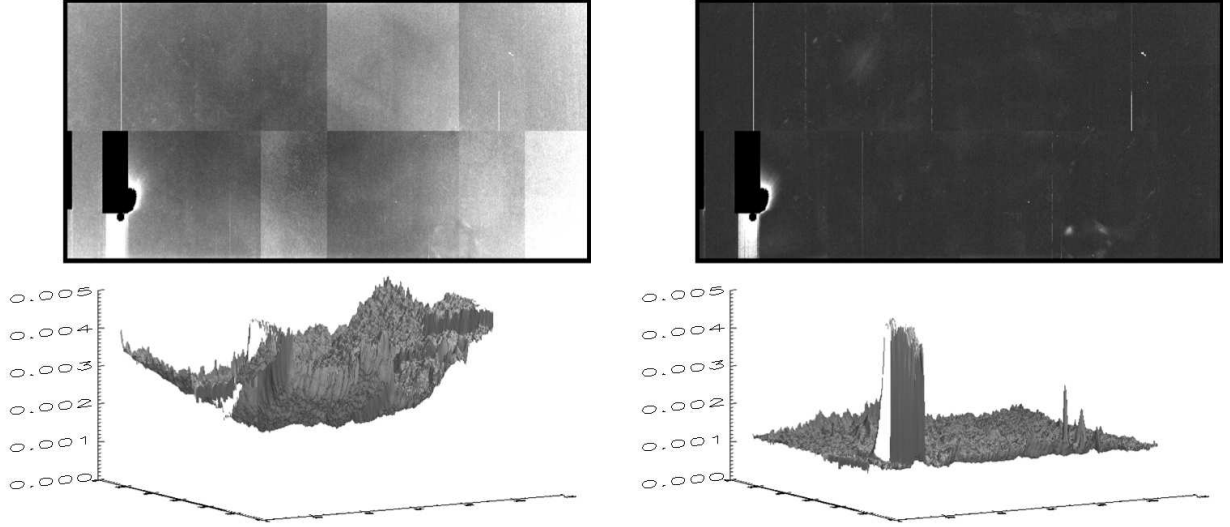


Figure 5. Left: 2D and 3D plots of the master flat RMS image without gradient correction. Right: 2D and 3D plots of the master flat RMS image with gradient correction (channel fitting). The black regions in the lower-left part of each image are the bad pixels which were masked. The high RMS pixels near those black regions are affected by electron overflow from the bad pixels.

5. STRATEGY FOR TAKING FLAT-FIELD

Based on our experiments and results, we suggest the following strategy for taking the sky flat-field images in order to achieve more flatness and high accuracy for wide-field telescope.

- 1) Determine the start and end time of taking the flat-field images by calculating the local altitude of the Sun;
- 2) Point the telescope toward the null point where the sky brightness gradient is minimal (towards anti-sun direction, altitude 75 degrees);
- 3) Take a short-exposure image to determine the zero point of the sky brightness in eq. 1 for that date;
- 4) Calculate the exposure time based on eq. 1, which provides the relationship between the sky brightness and the solar altitude.
- 5) Take flat-field images with tracking;
- 6) After about 30 seconds of multiple exposures or a single exposure longer than 30 seconds, point the telescope back toward the null point again, and repeat steps 4 and 5.

Based on the above observing strategy, we have developed a program to take flat-field images automatically. The automated program improves the efficiency and accuracy of flat-field taking during the limited twilight time for each day.

6. CONCLUSIONS

We have studied the sky flat-field images of the wide-field telescope AST3-1 from the observation in 2012 at Dome A, Antarctica. We have developed the relationships between local solar position, telescope pointing direction, and the flux and gradients of sky brightness. We have found that a 1% level of the gradient within our field of view is hard to avoid even if the telescope is pointed to the null point where the gradient of sky brightness is minimum and stable. This gradient will have impacts on photometric accuracy and stability which are especially critical to the time domain astronomy. We tested various fitting methods to remove the gradient in each individual flat-field frames before combination. The optimal method could reduce spatially dependent errors in the combined master flat-field to the negligible level.

Based on the real-time sky brightness distribution, we have optimized the twilight flat-field acquisition and suggested an automatic flat-field observing procedure in order to observe a more stable and uniform sky. With this observational strategy we can minimize the nonuniformity of light source. Our optimized flat-fielding not only improves the image quality and photometric accuracy for achieving the scientific goals of AST3, but will also provide scientific evidence and guidance of flat-fielding for other wide-field robotic autonomous telescopes.

ACKNOWLEDGMENTS

This work has been supported by the National Basic Research Program of China (973 Program) under grand No. 2013CB834900, the Chinese Polar Environment Comprehensive Investigation & Assessment Programmes under grand No. CHINARE2014-02-03, and the National Natural Science Foundation of China under grant No. 11003027, 11203039, and 11273019.

REFERENCES

- [1] Chromey, F. R. and Hasselbacher, D. A., “The Flat Sky: Calibration and Background Uniformity in Wide Field Astronomical Images,” *PASP* **108**, 944 (Oct. 1996).
- [2] Freudling, W., Romaniello, M., Patat, F., Møller, P., Jehin, E., and O’Brien, K., “Photometry with FORS at the ESO VLT,” in [*The Future of Photometric, Spectrophotometric and Polarimetric Standardization*], Sterken, C., ed., *Astronomical Society of the Pacific Conference Series* **364**, 113 (Apr. 2007).
- [3] Tyson, N. D. and Gal, R. R., “An exposure guide for taking twilight flatfields with large format CCDs,” *AJ* **105**, 1206–1212 (Mar. 1993).
- [4] Zhou, X., Burstein, D., Byun, Y.-I., Chen, J.-S., Chen, W.-P., Jiang, Z.-J., Ma, J., Sun, W.-H., Windhorst, R. A., Wu, H., Xu, W., and Zhu, J., “Dome-Diffuser Flat-fielding for Schmidt Telescopes,” *AJ* **127**, 3642–3652 (June 2004).
- [5] Cui, X., Yuan, X., and Gong, X., “Antarctic Schmidt Telescopes (AST3) for Dome A,” *Proc. SPIE* **7012**, 70122D (2008).
- [6] Yuan, X., Cui, X., Gong, X., Wang, D., Yao, Z., Li, X., Wen, H., Zhang, Y., Zhang, R., Xu, L., Zhou, F., Wang, L., Shang, Z., and Feng, L., “Progress of Antarctic Schmidt Telescopes (AST3) for Dome A,” *Proc. SPIE* **7733**, 77331V (2010).
- [7] Li, Z., Yuan, X., Cui, X., Wang, D., Gong, X., Du, F., Zhang, Y., Hu, Y., Wen, H., Li, X., Xu, L., Shang, Z., and Wang, L., “Status of the first Antarctic survey telescopes for Dome A,” *Proc. SPIE* **8444**, 84441O (2012).
- [8] Patat, F., Ugolnikov, O. S., and Postlyakov, O. V., “UBVRI twilight sky brightness at ESO-Paranal,” *AAP* **455**, 385–393 (Aug. 2006).